Frontiers of Information Technology & Electronic Engineering
www.zju.edu.cn/jzus; engineering.cae.cn; www.springerlink.com
ISSN 2095-9184 (print); ISSN 2095-9230 (online)
E-mail: jzus@zju.edu.cn

An analysis in metal barcode label design for reference*

Yin ZHAO†, Hong-guang XU, Qin-yu ZHANG†‡

(*Communication Engineering Research Center, Harbin Institute of Technology Shenzhen Graduate School, Shenzhen 518055, China*)

†E-mail: zhaoyin214@qq.com; zqy@hit.edu.cn

Received July 7, 2015; Revision accepted Nov. 23, 2015; Crosschecked Jan. 6, 2016

Abstract: We employ nondestructive evaluation involving AC field measurement in detecting and identifying metal barcode labels, providing a reference for design. Using the magnetic scalar potential boundary condition at notches in thin-skin field theory and 2D Fourier transform, we introduce an analytical model for the magnetic scalar potential induced by the interaction of a high-frequency inducer with a metal barcode label containing multiple narrow saw-cut notches, and then calculate the magnetic field in the free space above the metal barcode label. With the simulations of the magnetic field, qualitative analysis is given for the effects on detecting and identifying metal barcode labels, which are caused by metal material, notch characteristics, exciting inducer properties, and other factors that can be used in metal barcode label design as reference. Simulation results are in good accordance with experiment results.

Key words: Metal barcode label, Signal detection, AC field measurement, Internet of things
http://dx.doi.org/10.1631/FITEE.1500212 **CLC number:** O441.5

1 Introduction

The Internet of things (IoT) (Presser *et al.*, 2009), i.e., the network of physical objects or 'things', has been widely used in network convergence, via communication and sensing technology such as intelligent perception, recognition, and pervasive computing. As a basic support technique of IoT, recognition employs mainly the barcode, the magnetic card, or radio frequency identification (RFID). However, the above techniques are not suitable for working in harsh environments, such as in industry, automation, and control. What is worse, it is hard to identify small metal objects using these techniques.

The metal barcode label (MBL) is a special barcode that is engraved in the metal substrate with a laser beam etcher. It has the advantages of: (1) surviving in hostile environments and weather such as corrosion, high and low temperature, and ultraviolet (UV) fading; (2) long-term storage outdoors and being hard to damage; (3) high anti-interference; and (4) aging resistance. Therefore, an MBL is suitable for working in industry and military, e.g., petroleum and chemical industry, chain super catering industry, automation, detection, automatic administration, machinery production, electronics, medical apparatus, pressure vessel, arms, ammunition, and storage management. Generally, two kinds of MBL, namely metal tags (MTs) and direct park marking (DPM), have been widely used. For MT, the barcode is engraved in a separate metal substrate, and for DPM, the barcode is engraved directly on the goods. Traditionally, MBLs can be identified by a general barcode reader and/or techniques based on image recognition. However, the main drawback of these reading techniques is that they are hypersensitive to stain and, therefore, MBLs must be cleaned when they are stained by oil or dust. To overcome this drawback, one can adopt the eddy current (EC) effect to recognize MBLs, which is widely used in

‡ Corresponding author
* Project supported by the National Natural Science Foundation of China (No. 61271247)
ORCID: Yin ZHAO, http://orcid.org/0000-0002-6300-5939

nondestructive evaluation (NDE).

However, only a few papers have reported MBLs until today. In these papers, the analysis is based on the equivalent impendence equation derived from the Kirchhoff voltage law:

$$Z_{\mathrm{L}} = R_1 + R_2 \frac{\omega^2 M^2}{R_2^2 + \omega^2 L_2^2} + \mathrm{j}\omega \left(L_1 - L_2 \frac{\omega^2 M^2}{R_2^2 + \omega^2 L_2^2} \right), \tag{1}$$

where R_1 and R_2 are the resistances of the exciting and pick-up coils, respectively, L_1 and L_2 the self-inductances of the exciting and pick-up coils, respectively, and M the mutual inductance of the exciting and pick-up coils. From Eq. (1), one cannot obtain the effects of metal substrate conductivity or permeability, the depth of notches, the shape or size of exciting coils, exciting current magnitude, frequency, lift-off distance, etc., on identifying MBLs.

In this study, the information contained in an MBL is recorded as information bits $b_1, b_2, \ldots, b_K$, which are arranged on the surface of the metal substrate separated by a distance Δy; a saw-cut notch is engraved on the metal substrate at the position where $b_k = 1$ ($k = 1, 2, \ldots, K$), while at the position where $b_k = 0$ there are no notch (Fig. 1).

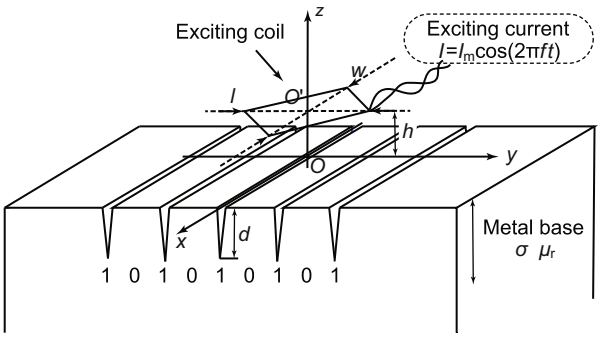

Fig. 1 Metal barcode label: schematic diagram

Because of the similarity between cracks in a specimen and notches in an MBL, one can intuitively extend the theory and techniques developed in NDE (Auld and Moulder, 1999; Grimberg, 2011) to the MBL field. NDE involves mainly eddy current testing (ECT) (Bowler and Harfield, 1998; Ditchburn *et al.*, 2003; Grimberg, 2011) and AC field measurement (ACFM) (Mirshekar-Syahkal and Mostafavi, 1997; Mostafavi and Mirshekar-Syahkal, 1999; Zhou *et al.*, 1999; Salemi *et al.*, 2004; Amineh *et al.*, 2008). For some special cases in which cracks are ideal and/or have a special shape, analytical and semi-analytical solutions have been obtained (Dodd and Deeds, 1968; Bowler *et al.*, 1990; Bowler, 1994; Bowler and Harfield, 1998; Ditchburn *et al.*, 2003; Theodoulidis and Bowler, 2005; 2010; Ostovarzadeh *et al.*, 2011; 2013; Bowler *et al.*, 2012), while for much more general cases numerical methods such as volume integrals (Bowler *et al.*, 1989) and the finite element method (FEM) (Morisue, 1982; French and Bond, 1988; Xu and Simkin, 2004; Zeng *et al.*, 2007; 2010) are necessary. In this paper, we provide an analytical model to analyze and predict the effects of metal substrate conductivity and permeability, the properties of notches and exciting coils, etc., on identifying MBLs, by employing the analysis technique for ACFM (Mirshekar-Syahkal and Mostafavi, 1997) and the boundary equations in the thin-skin electromagnetic field (Lewis *et al.*, 1988; Michael *et al.*, 1991), whose skin depth δ is much smaller compared to the dimensions of notches. The analytical solutions for the magnetic scalar potential corresponding to the perturbations caused by multiple narrow saw-cut notches are given, which can be used to extract the information bits from MBLs. Computer simulation demonstrates that the results are in good accordance with those of experiments. With this model, we can qualitatively analyze the effects of metal substrate conductivity and permeability, the properties of notches and exciting coils, etc., on identifying MBL, and provide a reference for designing MBLs.

2 Theoretical modeling

The considered problem is shown schematically in Fig. 1, where a half-space uniform metal substrate with conductivity σ and relative permeability μ_{r} is shown, whose surface coincides with the plane $z = 0$. N narrow saw-cut notches with infinite length and depth d are taken to be parallel to the x-axis at positions $y_1, y_2, \ldots, y_N$ ($y_1, y_2, \ldots, y_N$ are integer multiples of Δy), respectively. An exciting coil, with center point $(0, 0, h)$, is placed parallel to the surface of the metal substrate. The exciting coil carries an alternating current with magnitude I_{m} and operating frequency f. The operating frequency ranges from 10 kHz to 10 MHz, such that the induced displacement current can be neglected, and the current skin depth $\delta = \sqrt{2}/|k|$ ($k^2 = \mathrm{j}2\pi f \mu_0 \mu_{\mathrm{r}} \sigma$, $\mathrm{Re}(k)>0$, where μ_0 is the vacuum permeability and $\mathrm{Re}(k)$ the real part

of k) is much smaller than the dimensions of the notches. The field magnitude is so small compared with the saturation field that magnetic hysteresis can also be neglected (Michael *et al.*, 1991). The shape of the exciting coil can be either circular or rhombic. A pick-up coil, with a lift-off distance q, is placed with its axis in the yOz plane and parallel to the y-axis, to collect the y component of the magnetic field $\boldsymbol{H}$ in free space.

2.1 Scalar magnetic potential in free space

In free space, the vector magnetic potential induced by the current density $\boldsymbol{J}(\boldsymbol{r}_0)$ is established as

$$\boldsymbol{A}_{\mathrm{i}}(\boldsymbol{r}) = \frac{\mu_0}{4\pi}\iiint_{\Omega_{\mathrm{src}}} \frac{\boldsymbol{J}(\boldsymbol{r}_0)}{|\boldsymbol{r}-\boldsymbol{r}_0|}\mathrm{d}^3\boldsymbol{r}_0, \tag{2}$$

where $\boldsymbol{r}_0$ and $\boldsymbol{r}$ are the source and field points, respectively, and Ω_{src} is the source domain. Its 2D Fourier transform is given by (Michael *et al.*, 1982)

$$\begin{aligned}\tilde{\tilde{\boldsymbol{A}}}_{\mathrm{i}}(\alpha,\beta,z) &= \frac{\mu_0}{4\pi\gamma}\\ &\times \iiint_{\Omega_{\mathrm{src}}} \boldsymbol{J}(\boldsymbol{r}_0)\exp\left(-\mathrm{j}(\alpha x_0+\beta y_0)\right.\\ &\left.-\gamma|z-z_0|\right)\mathrm{d}x_0\mathrm{d}y_0\mathrm{d}z_0,\end{aligned} \tag{3}$$

where $\gamma=\sqrt{\alpha^2+\beta^2}$, $\boldsymbol{r}_0 = x_0\boldsymbol{e}_x + y_0\boldsymbol{e}_y + z_0\boldsymbol{e}_z$, and $\tilde{\tilde{\cdot}}$ denotes the 2D Fourier transform of a function with respect to x and y. When the inducer is a current-carrying coil, Eq. (3) is simplified to

$$\begin{aligned}\tilde{\tilde{\boldsymbol{A}}}_{\mathrm{i}}(\alpha,\beta,z) &= \frac{\mu_0 I}{4\pi\gamma}\\ &\times \oint_c \exp\left(-\mathrm{j}(\alpha x_0+\beta y_0)-\gamma|z-z_0|\right)\mathrm{d}\boldsymbol{l}_0,\end{aligned} \tag{4}$$

where $I = I_{\mathrm{m}}\cos(2\pi f t)$ is the current in the coil, c is the integration path along the coil, and $\mathrm{d}\boldsymbol{l}_0$ is a vector line element. Approximating the exciting coil by M short segments of conductors (Fig. 1), one can use the well-known expression for vector magnetic field to obtain (Ravan *et al.*, 2006)

$$\begin{aligned}\tilde{\tilde{\boldsymbol{A}}}_{\mathrm{i}}(\alpha,\beta,0) = \frac{\mu_0 I}{4\pi\gamma}\sum_{i=1}^{M}\Bigg(&\frac{\exp(-\mathrm{j}(\alpha x_{0,i}+\beta y_{0,i})-\gamma z_{0,i})}{-\mathrm{j}(\alpha \mathrm{L}x_{0,i}+\beta \mathrm{L}y_{0,i})-\gamma \mathrm{L}z_{0,i}}\\ &\times\left(\exp(-\mathrm{j}(\alpha \mathrm{L}x_{0,i}+\beta \mathrm{L}y_{0,i})-\gamma \mathrm{L}z_{0,i})-1\right)\\ &\times\left(\mathrm{L}x_{0,i}\boldsymbol{e}_x+\mathrm{L}y_{0,i}\boldsymbol{e}_y+\mathrm{L}z_{0,i}\boldsymbol{e}_z\right)\Bigg),\end{aligned} \tag{5}$$

where $x_{0,i}$, $y_{0,i}$, and $z_{0,i}$ are the starting coordinates of the ith segment of the conductor, $\mathrm{L}x_{0,i} = x_{0,i+1} - x_{0,i}$, $\mathrm{L}y_{0,i} = y_{0,i+1} - y_{0,i}$, and $\mathrm{L}z_{0,i} = z_{0,i+1} - z_{0,i}$.

In the region Ω_{air} (above the metal substrate surface, outside the notches, and below the exciting coil) which we are interested in, the magnetic field is divergence- and curl-free, i.e., $\nabla\times\boldsymbol{H}=0$, $\nabla\cdot\boldsymbol{H}=0$, and can be derived from a scalar magnetic potential ψ by using $\boldsymbol{H}=-\nabla\psi$. The scalar magnetic potential can be expressed as the superposition of two potentials with Laplacian distributions as

$$\psi = \psi_{\mathrm{i}} + \psi_{\mathrm{p}}, \tag{6}$$

where ψ_{i} and ψ_{p} are the potential functions for the incident field in the absence of the metal and the field perturbations caused by the metal substrate and the notches, respectively. The boundary condition that ψ satisfies in the case of a single notch has been given by Lewis *et al.* (1988) and Michael *et al.* (1991). In this study, the boundary condition is modified to fit the case of N notches as on the plane $z=0$:

$$\begin{aligned}&\frac{\mu}{k}\nabla_{\mathrm{t}}^2\psi + \mu_0\frac{\partial\psi}{\partial z}\\ &= -\left(\frac{2\mu}{k}+\mu_0 g\right)\sum_{n=1}^{N} H_z(x,y_n,0)\delta(y-y_n),\end{aligned} \tag{7}$$

where $H_z(x,y_n,0)$ is the magnetic field at the nth notch on the surface of the specimen. Note that the boundary condition in Eq. (7) is available only for the case where the notch opening is sufficiently small, so $H_z(x,y_n,0)$ has a negligible variation inside the notch from one face to the other for an arbitrary incident field distribution (Ravan *et al.*, 2006). The Fourier transform of Eq. (7) is

$$\begin{aligned}&-\frac{\mu}{k}\gamma^2\tilde{\tilde{\psi}}(\alpha,\beta,0) + \mu_0\left.\frac{\partial\tilde{\tilde{\psi}}(\alpha,\beta,z)}{\partial z}\right|_{z=0}\\ &= -\left(\frac{2\mu}{k}+\mu_0 g\right)\sum_{n=1}^{N}\tilde{H}_z(\alpha,y_n,0)\exp(-\mathrm{j}\omega y_n).\end{aligned} \tag{8}$$

Using Eq. (3) and the 2D Fourier transform of the well-known relations $\boldsymbol{B}_{\mathrm{i}} = \nabla\times\boldsymbol{A}_{\mathrm{i}}$ and $\boldsymbol{H}_{\mathrm{i}} = -\nabla\psi_{\mathrm{i}}$, the Fourier transform of the incident potential ψ_{i} in Ω_{air} is given by (Mirshekar-Syahkal and Mostafavi, 1997)

$$\tilde{\tilde{\psi}}_{\mathrm{i}}(\alpha,\beta,z) = \tilde{\tilde{\psi}}_{\mathrm{i}}(\alpha,\beta,0)\mathrm{e}^{\gamma z},\ z<h, \tag{9}$$

$$\tilde{\tilde{\psi}}_{\mathrm{i}}(\alpha,\beta,0) = \frac{1}{\mathrm{j}\mu_0\gamma}\boldsymbol{e}_z\cdot\left(\boldsymbol{\gamma}\times\tilde{\tilde{\boldsymbol{A}}}_{\mathrm{i}}(\alpha,\beta,0)\right), \tag{10}$$

where $\boldsymbol{\gamma}=\alpha\boldsymbol{e}_x+\beta\boldsymbol{e}_y$. The perturbation potential ψ_p in Eq. (6) satisfies the Laplacian equation $\nabla^2\psi_\mathrm{p}=0$, and the general solution is given by

$$\tilde{\tilde{\psi}}_\mathrm{p}(\alpha,\beta,z)=a\exp(-\gamma z), \tag{11}$$

where a is a coefficient and will be determined later in this article. The 2D Fourier transform of the total potential $\tilde{\tilde{\psi}}(\alpha,\beta,z)$ is obtained by the superposition of Eqs. (9) and (11):

$$\tilde{\tilde{\psi}}(\alpha,\beta,z)=\tilde{\tilde{\psi}}_\mathrm{i}(\alpha,\beta,0)\exp(\gamma z)+a\exp(-\gamma z). \tag{12}$$

Substituting Eq. (12) with $z=0$ in Eq. (8), one can obtain

$$\begin{aligned}\tilde{\tilde{\psi}}(\alpha,\beta,0)=&\frac{2\mu_0\gamma\tilde{\tilde{\psi}}_\mathrm{i}(\alpha,\beta,0)}{\gamma\left(\mu_0+\dfrac{\mu}{k}\gamma\right)}\\&+\frac{\left(2\dfrac{\mu}{k}+\mu_0 g\right)\displaystyle\sum_{n=1}^{N}\tilde{H}_z(\alpha,y_n,0)\exp(-\mathrm{j}\beta y_n)}{\gamma\left(\mu_0+\dfrac{\mu}{k}\gamma\right)}.\end{aligned} \tag{13}$$

Inside the nth notch ($y=y_n$) between its two faces, the scalar magnetic potential ϕ satisfies the Laplacian equation $\nabla^2\phi=0$. Since the notch opening is sufficiently small, the boundary condition corresponds to no tangential current along the inside notch edge (Michael *et al.*, 1991) (Fig. 2), i.e.,

$$J_x(x,y_n,-d)=0, \tag{14}$$

which means no normal magnetic field along the inside notch edge:

$$H_y(x,y_n,-d)=-\frac{\partial\phi(x,y_n,-d)}{\partial y}=0. \tag{15}$$

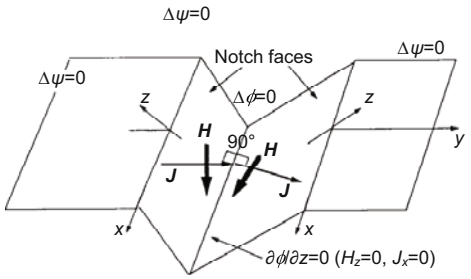

Fig. 2 Magnetic field inside the nth notch and the current at the nth notch face (Mirshekar-Syahkal and Mostafavi, 1997)

Since the nth notch is infinitely long, the 1D Fourier transform solution for $\nabla^2\phi=0$ is given by

$$\tilde{\phi}(\alpha,y_n,z)=C\frac{\cosh[\alpha(z+d)]}{\cosh(\alpha d)}, \tag{16}$$

$$\tilde{H}_z(\alpha,y_n,0)=-\alpha C\tanh(\alpha d), \tag{17}$$

where "~" denotes the 1D Fourier transform solution with respect to x. With Eqs. (16) and (17), $\tilde{\phi}(\alpha,y_n,z)$ can be expressed in terms of $\tilde{H}_z(\alpha,y_n,0)$ as

$$\tilde{\phi}(\alpha,y_n,z)=\frac{-1}{\alpha\tanh(\alpha d)}\frac{\cosh[\alpha(z+d)]}{\cosh(\alpha d)}\tilde{H}_z(\alpha,y_n,0). \tag{18}$$

Because of the continuity of the potentials ϕ and ψ, their 1D Fourier transforms are equal at the crack mouth:

$$\tilde{\phi}(\alpha,y_n,0)=\tilde{\psi}(\alpha,y_n,0). \tag{19}$$

Combining Eqs. (19), (18), and (13), one can obtain the relationship between the z component of the magnetic field and the incident potential ψ_i on the surface of the metal substrate at the nth notch ($y=y_n$) as follows:

$$\begin{aligned}&\sum_{m=1}^{N}\left[\left(\alpha\tanh(\alpha d)\left(2\frac{\mu_\mathrm{r}}{k}+g\right)\right.\right.\\&\quad\left.\times\int_{-\infty}^{\infty}\frac{\exp(-\mathrm{j}\beta(y_m-y_n))}{\gamma\left(1+\dfrac{\mu_\mathrm{r}}{k}\gamma\right)}\mathrm{d}\beta+\sqrt{2\pi}\delta_{mn}\right)\\&\quad\left.\times\tilde{H}_z(\alpha,y_m,0)\right]\\&=-2\alpha\tanh(\alpha d)\int_{-\infty}^{\infty}\frac{\tilde{\tilde{\psi}}_\mathrm{i}(\alpha,\beta,0)}{1+\dfrac{\mu_\mathrm{r}}{k}\gamma}\exp(\mathrm{j}\beta y_n)\mathrm{d}\beta.\end{aligned} \tag{20}$$

Eq. (20) can be rewritten in a matrix form as

$$\left(\boldsymbol{A}+\sqrt{2\pi}\boldsymbol{I}\right)\tilde{\boldsymbol{H}}_z=\boldsymbol{B}, \tag{21}$$

where $\boldsymbol{I}$ is the identity matrix and the elements in $\boldsymbol{A}$, $\boldsymbol{B}$, and $\tilde{\boldsymbol{H}}_z$ are, respectively,

$$a_{nm}=\alpha\tanh(\alpha d)\left(2\frac{\mu_\mathrm{r}}{k}+g\right)\int_{-\infty}^{\infty}\frac{\exp(-\mathrm{j}\beta(y_m-y_n))}{\gamma\left(1+\dfrac{\mu_r}{k}\gamma\right)}\mathrm{d}\beta, \tag{22}$$

$$b_n=-2\alpha\tanh(\alpha d)\int_{-\infty}^{\infty}\frac{\tilde{\tilde{\psi}}_\mathrm{i}(\alpha,\beta,0)}{1+\dfrac{\mu_\mathrm{r}}{k}\gamma}\exp(\mathrm{j}\beta y_n)\mathrm{d}\beta, \tag{23}$$

$$\tilde{H}_{z,m} = \tilde{H}_z(\alpha, y_m, 0), \tag{24}$$

and

$$\tilde{\boldsymbol{H}}_z = \left(\boldsymbol{A} + \sqrt{2\pi}\boldsymbol{I}\right)^{-1} \boldsymbol{B}. \tag{25}$$

Now, using Eqs. (12), (13), and (20), the 2D Fourier transform of the potential ψ above the metal surface can be obtained as

$$\begin{aligned}
&\tilde{\tilde{\psi}}(\alpha, \beta, z)\\
&= \tilde{\tilde{\psi}}_{\mathrm{i}}(\alpha, \beta, 0)\mathrm{e}^{\gamma z} + \frac{1 - \dfrac{\mu_{\mathrm{r}}}{k}\gamma}{1 + \dfrac{\mu_{\mathrm{r}}}{k}\gamma}\tilde{\tilde{\psi}}_{\mathrm{i}}(\alpha, \beta, 0)\mathrm{e}^{-\gamma z}\\
&+ \frac{2\dfrac{\mu_{\mathrm{r}}}{k} + g}{\gamma\left(1 + \dfrac{\mu_{\mathrm{r}}}{k}\gamma\right)}\left(\sum_{n=1}^{N} \tilde{H}_z(\alpha, y_n, 0)\exp(-\mathrm{j}\beta y_n)\right)\mathrm{e}^{-\gamma z}.
\end{aligned} \tag{26}$$

The second and third terms on the right-hand side of Eq. (26) are the potential functions corresponding to the perturbations caused by the metal and the notches, respectively. It is clear that $\tilde{\tilde{\psi}}(\alpha, \beta, z)$ is a function of the incident potential at the metal surface, $\tilde{\tilde{\psi}}_{\mathrm{i}}(\alpha, \beta, 0)$, which can be obtained by using $\tilde{\tilde{\boldsymbol{A}}}_{\mathrm{i}}(\alpha, \beta, 0)$ (Eq. (10)). Applying 2D inverse Fourier transform to Eq. (26), one can obtain the total potential function in Ω_{air}, $\psi(x, y, z)$, and with the definition of the scalar magnetic potential, the y component of the magnetic field, H_y, can be obtained.

2.2 Qualitative analysis for sensitivity

In this study, the physical quantity measured by the ACFM pick-up coil is the y component of the magnetic field in Ω_{air}, i.e.,

$$\begin{aligned}
H_y(x, y, z) &= -\frac{\partial \psi_{\mathrm{i}}(x, y, z)}{\partial y} - \frac{\partial \psi_{\mathrm{p,specimen}}(x, y, z)}{\partial y}\\
&\quad - \sum_{n=1}^{N} \frac{\partial \psi_{\mathrm{p,notch},n}(x, y, z)}{\partial y}\\
&= H_{y,\mathrm{inherent}} + \sum_{n=1}^{N} H_{y,\mathrm{notch},n}.
\end{aligned} \tag{27}$$

The first two terms on the right-hand side of Eq. (27) are the y components of the inherent magnetic field caused by the exciting coil and the metal substrate, $H_{y,\mathrm{inherent}}$, and the third one is the superposition of the perturbation magnetic field caused by notches, $H_{y,\mathrm{notch},n}$. In view of Eqs. (20), (21), and (26), the perturbation potential caused by the nth notch, $\psi_{\mathrm{p,notch},n}$, can be approximated by a linear combination of $\psi_{\mathrm{i}}(x, y, z)$, the same as $H_{y,\mathrm{notch},n}$ to the y component of the incident magnetic field, $H_{y,\mathrm{i}}$. The sensitivity of the pick-up coil depends on two factors: (1) the main lobe width of the perturbation magnetic field caused by the nth notch, $H_{y,\mathrm{notch},n}$, and (2) the relative perturbation magnetic field caused by the nth notch, $\max\left(|H_{y,\mathrm{notch},n}|\right) / \max(|H_{y,\mathrm{inherent}}|)$.

The effects of the metal substrate's conductivity and permeability, the properties of notches and exciting coils, etc., on identifying MBL will be given in the following section by simulations.

3 Simulations

The sensitivity in identifying MBLs depends on the metal substrate material, the properties of notches, and exciting coils. In this section, a qualitative analysis of the sensitivity in identifying MBLs containing a single notch by examining the magnetic field distribution in Ω_{air}, is given first. Then according to the conclusions obtained above, a set of recommended parameters are given in the case of MBLs containing multiple notches, which can be used in designing MBLs.

In addition, this technique can be very effective (almost instantaneous running on a personal computer) for the magnetic vector potential $\tilde{\tilde{\boldsymbol{A}}}_{\mathrm{i}}(\alpha, \beta, 0)$ induced by the exciting coils, which is the most time-consuming process and is performed only once in the entire simulation.

3.1 Identification of single-notch MBLs

The parameters used in the simulations (Experiments 1–6) for the MBLs containing a single notch are summarized in Table 1.

In Experiment 1, the identification of the MBLs containing a single notch (bit 1) or no notch (bit 0) with mild steel or aluminum substrates is investigated. A rhombic coil (diagonals l=21.5 mm, w=11.5 mm) with current of an operating frequency f=20 kHz is used for exciting. Fig. 3 gives the magnitude and phase of the y component of the magnetic fields obtained by simulation and experiment (Mirshekar-Syahkal and Mostafavi, 1997) along the pick-up coil's moving path (the intersection of planes x=0 and z=q). It is seen that (1) the simulation results are in good agreement with the

Table 1 Parameters used in the simulations for MBLs containing a single notch

Experiment	Metal substrate material	Shape of the exciting coil	Operating frequency, f (kHz)	Lift-off distance, q (mm)	Notch depth, d (mm)	Notch position, y_n (mm)	Simulation results
1	Mild steel	Small rhombic coil	20	0.76	–	–	Fig. 3
	Aluminum				–	–	
	Mild steel				4	0	
	Aluminum				4	0	
2	Mild steel	Small rhombic coil	10	0.76	4	0	Fig. 4
			20				
			40				
3	Mild steel	Small rhombic coil	20	0.76	4	0	Fig. 5
						−4	
						−8	
						−12	
						−16	
4	Mild steel	Small rhombic coil	20	0.76	1	0	Fig. 6
					2		
					4		
					8		
					12		
					16		
5	Mild steel	Small rhombic coil	20	0.76	4	0	Fig. 7
		Large rhombic coil					
		Small circular coil					
		Large circular coil					
6	Mild steel	Small rhombic coil	20	0.38	4	0	Fig. 8
				0.76			
				1.14			
				1.52			
	Aluminum			0.38			
				0.76			
				1.14			
				1.52			

Properties of the metal substrate material: mild steel, μ_r=100, σ=6 × 10^6 S/m; aluminum, μ_r=1, σ=3.7 × 10^7 S/m. Exciting coil dimensions: small exciting rhombic coil, diagonals l=21.5 mm and w=11.5 mm; large exciting rhombic coil, diagonals l=43 mm and w=23 mm; small exciting circular coil, radii r=10.75 mm; large exciting circular coil, radii r=21.50 mm. The exciting coil is placed at z=3.16 mm (Fig. 1). Exciting current magnitude I_m=1 A. The notch has an opening g=150 μm

experiment when an MBL contains no notch; (2) the magnitude of H_y has a double peak pattern at the position around the notch position (y=0) and the phase flips over, which are the same as that in Mirshekar-Syahkal and Mostafavi (1997) and Salemi *et al.* (2004); (3) compared with a substrate with low permeability (aluminum), the relative perturbation in magnetic field, caused by a notch carved in a substrate with high permeability (mild steel), is larger. Therefore, a substrate with high permeability can improve the sensitivity of MBL's identification.

The identification of MBLs made of mild steel which contains a single notch placed at the position y=0 mm with depth d=4 mm, is investigated in Experiment 2. A rhombic coil (diagonals l=21.5 mm, w=11.5 mm) with current of operating frequencies f=10, 20, and 40 kHz, respectively, is used for exciting. Fig. 4 gives the magnitude of H_y along the pick-up coil's moving path. It is seen that (1) the magnitude of H_y increases as the operating frequency f increases, but the relative perturbation does not change significantly, and (2) the main lobe width of the perturbation in the magnitude of H_y, caused by a notch, is independent of the operating frequency f. It is known that the squared skin depth is inversely proportional to the operating frequency. Therefore, the change of the skin depth caused by the operating frequency alone influences the MBL's identification.

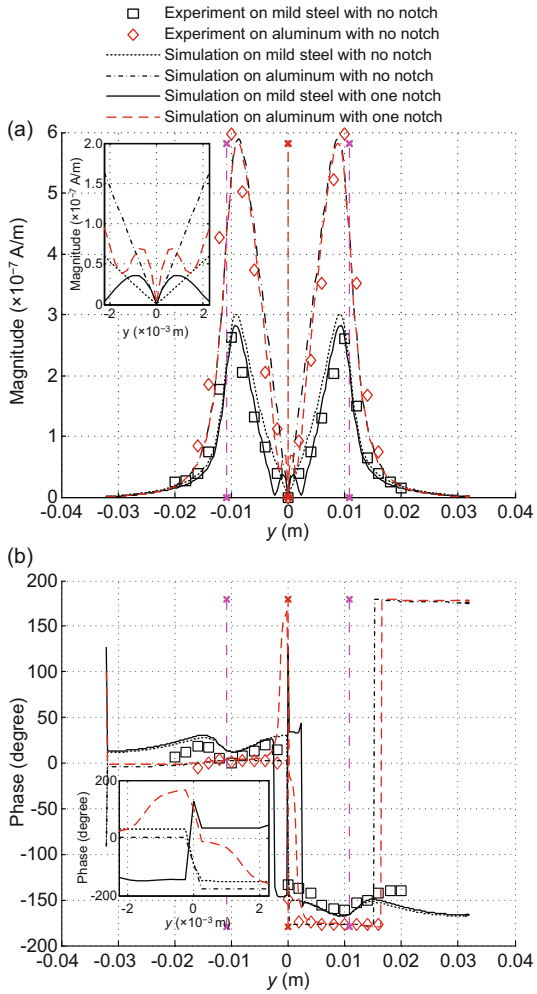

Fig. 3 Identification of MBLs containing a single notch or no notch: (a) magnitude; (b) phase. Simulation results of H_y are compared with experimental results given in Mirshekar-Syahkal and Mostafavi (1997). The subplots show the detailed H_y around y=0. The position of the notch is marked with vertical dashed line, and the position of the exciting coil is marked with vertical dash-dotted lines

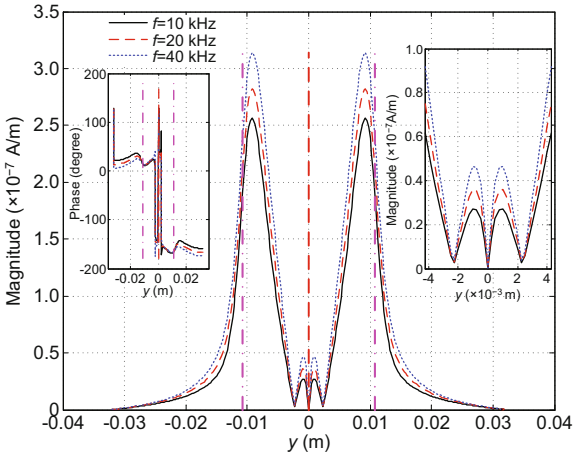

Fig. 4 Magnitude of H_y in identifying MBLs containing a single notch under different operating frequencies. The left subplot shows the phase of H_y, and the right subplot shows the detailed magnitude of H_y at the position of the notch. The position of the notch is marked with vertical dashed line, and the position of the exciting coil is marked with vertical dash-dotted lines

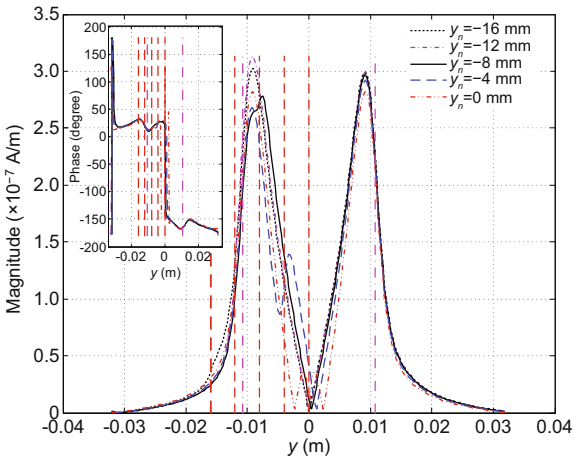

Fig. 5 Magnitude of H_y in identifying MBLs containing a single notch at different positions. The inset shows the phase of H_y. The position of the notch is marked with vertical dashed line, and the position of the exciting coil is marked with vertical dash-dotted lines

In Experiment 3, the identification of MBLs made of mild steel, containing a 4-mm-deep single notch with different positions, is investigated. The inducer is a rhombic coil with l=21.5 mm and w=11.5 mm and the operating frequency f is 20 kHz. Fig. 5 gives the magnitude and phase of the y component of the magnetic fields along the pick-up coil's moving path, obtained by simulation. From Fig. 5, we see the following: (1) When the notch is placed near the center of the exciting coil (y_n=−4 mm), there is a peak in the magnitude of H_y at the side close to the center of the exciting coil and a valley at the other side. In between the peak and valley is the position of the notch. However, the phase of H_y has a negligible variation at the notch. When y_n=0, the magnitude and phase of H_y are the same as shown in Fig. 3. Therefore, in this region, a notch can be positioned accurately. (2) When the notch is placed inside the exciting coil and near edges (y_n=−8 mm), the magnitude of H_y decreases significantly at the exciting coil's vertex near the notch (the left peak is much lower than the right one at the exciting coil vertexes), and the phase of H_y shows a negligible

variation at the notch. Therefore, one can detect the existence of a notch but cannot position it accurately. (3) When the notch is placed outside the exciting coil near edges (y_n=−12, −16 mm), both the magnitude and phase of H_y change negligibly at the notch. Therefore, a notch placed in this region cannot be detected. To improve the sensitivity of identifying MBLs, one should place notches in the center region of the exciting coil when manufacturing MBLs.

In Experiment 4, the identification of MBLs made of mild steel, containing a single notch placed at y=0 mm with different depths, is investigated. The inducer is a rhombic coil with l=21.5 mm and w=11.5 mm, and the operating frequency is f= 20 kHz. Fig. 6 gives the magnitude and phase of H_y along the pick-up coil's moving path, obtained by simulation. It is seen that (1) the double peaks of the H_y magnitude increase as the notch depth d increases at the beginning, but no more significant increase after d>8 mm, and (2) the main lobe width of the perturbation in the magnitude of the y component magnetic field, H_y, caused by a notch, increases as the notch depth d increases at the beginning, but no more significant increase after d>8 mm. Therefore, 4–8 mm is a good choice for the notch depth when manufacturing MBLs.

In Experiment 5, the identification of MBLs made of mild steel, containing a single notch placed at the position y_n=0 mm, depth d=4 mm, is investigated. The MBL is excited by rhombic and circular coils, respectively. The diagonals of small rhombic coils are l=21.5 mm, w=11.5 mm; for large rhombic coils, l=43 mm, w=23 mm. The radii of small circular coils are r=10.75 mm, and for large circular coils, r=21.5 mm. Fig. 7 gives the magnitude of H_y along the pick-up coil's moving path. It is seen that (1) the magnitude of H_y induced by a circular coil is higher than that induced by a rhombic one, but the relative perturbation caused by a notch is lower, and (2) the relative perturbation in the magnetic field caused by a notch increases as the size of exciting coils increases, but the main lobe width of the perturbation also increases. Therefore, for a fixed exciting coil, it is necessary to balance the sensitivity and the region in which notches can be detected when selecting the size of an exciting coil. To obtain a high sensitivity in identifying MBLs, one can scale the size of an exciting coil down and move it along the y-axis under the control of a computer. This is the future work of this study.

Tian *et al.* (1998) and Tian and Sophian (2005) have discussed the lift-off effects, such as normalization and material influence, on ECT with experiments. Following this discussion, in Experiment 6, the influence of the pick-up coil lift-off on the identification of MBLs is investigated. In this simulation, the MBL is made of mild steel and aluminum,

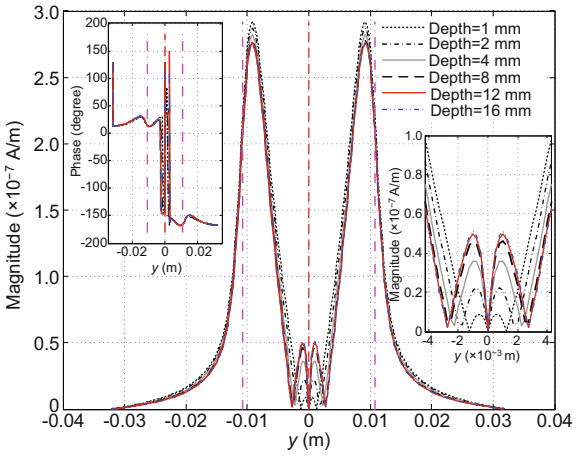

Fig. 6 Magnitude of H_y in identifying MBLs containing a single notch with different depths. The left inset shows the phase of H_y. The right inset shows the detailed magnitude of H_y at the position of the notch. The position of the notch is marked with vertical dashed line, and the position of the exciting coil is marked with vertical dash-dotted lines

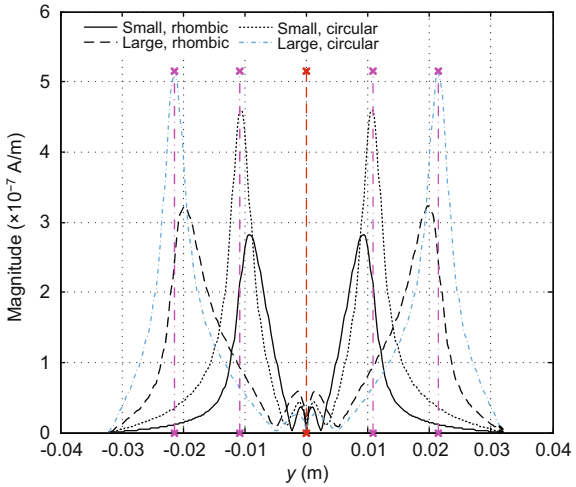

Fig. 7 Magnitude of H_y in identifying MBLs containing a single notch under exciting inducers with different shapes and sizes. The position of the notch is marked with vertical dashed line, and the position of the exciting coil is marked with vertical dash-dotted lines

respectively; the inducer is a rhombic coil with l=21.5 mm and w=11.5 mm; and the operating frequency is f=20 kHz. The pick-up coil lift-off q is fixed at 0.38, 0.76, 1.14, and 1.52 mm, respectively. Fig. 8 gives the normalized magnitude of H'_y along the pick-up coil's moving path at different lift-offs. The inset shows H'_y in detail at the position of the notch. The normalized signal H'_y is given by (Tian and Sophian, 2005)

$$H'_y = \frac{H_y}{\max(H_y)}. \tag{28}$$

As the lift-off increases, the normalized magnetic field decreases rapidly. In fact, as the pick-up coil is brought close to the substrate and far from the exciting coil, the magnetic field induced by the exciting coil increases substantially and that by the notch decreases obviously. According to Eq. (26), the dependence of the magnetic scalar potential ψ on z shows that the perturbation induced by notches decreases exponentially as the lift-off increases. Therefore, when the position of the exciting coil is fixed, it is obvious that the pick-up coil should be placed close to MBLs as much as possible.

As discussed in Section 2.2, the perturbation potential caused by the nth notch, $\psi_{\mathrm{p,notch},n}$, can be approximated as a linear combination of $\psi_{\mathrm{i}}(x,y,z)$,

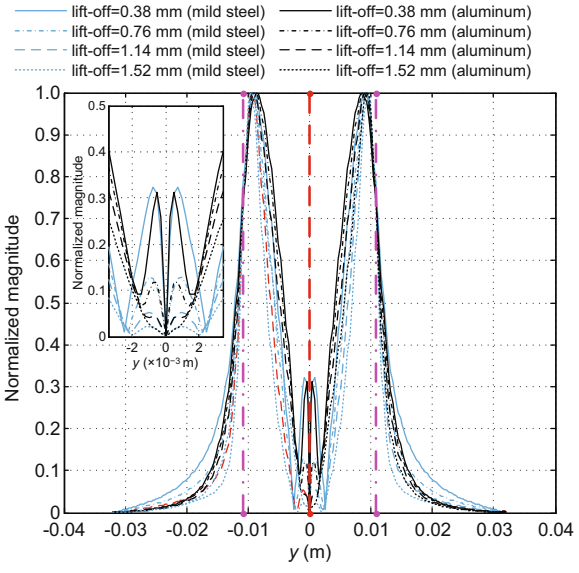

Fig. 8 Normalized magnitude of H_y in identifying MBLs containing a single notch with different lift-offs. The inset shows the detailed normalized magnitude of H_y at the position of the notch. The position of the notch is marked with vertical dashed line, and the position of the exciting coil is marked with vertical dash-dotted lines

the same as $H_{y,\mathrm{notch},n}$ to $H_{y,\mathrm{i}}$. By the simulations for MBLs containing a single notch, with different substrate materials and properties of notches and exciting coils (Figs. 3 and 4), it is known that the y component of the perturbed magnetic field caused by a single notch, $H_{y,\mathrm{notch},n}$, can be approximately depicted as a copy of $H_{y,\mathrm{inherent}}$, which is scaled down in magnitude, reversed in phase, and compressed in main lobe width. Mirshekar-Syahkal and Mostafavi (1997) suggested that phase detection is better than magnitude detection for detecting notches, because the perturbation in magnitude of H_y caused by the notch is much smaller than the peaks of H_y at the position of the exciting coil, while the perturbation in phase of H_y is obvious at the position of the notch. However, this suggestion is fit only when the notch is placed at y_n=0. From Fig. 5, it is known that, in case the position of the notch is at $y_n \neq 0$, the perturbation in phase is not obvious any more, and this is due to the fact that the relative perturbation in magnitude caused by the notch is much smaller than 1. Only at the position y_n=0 where the inherent magnetic field $H_{y,\mathrm{inherent}}$ is almost zero, the perturbation is predominant. So, Eq. (27) can be simplified as $H_y \approx H_{y,\mathrm{notch},n}|_{y_n=0}$, whose phase is opposite to the inherent phase. When the position of the notch $y_n \neq 0$, the inherent field $H_{y,\mathrm{inherent}}$ is much larger than $H_{y,\mathrm{notch},n}$ in magnitude, and the phase of $H_{y,\mathrm{notch},n}$ flips over at $y = y_n$, which is the same as that of $H_{y,\mathrm{inherent}}$ at the side near the coil center and opposite at the other side; hence, in the magnitude of H_y at $y = y_n$, a peak appears at the side near the coil center and a valley at the other side.

Therefore, to improve the sensitivity of the notch identification, one can conclude that (1) the magnitude detection should be employed in positioning notches with the ACFM technique; (2) the metal substrate should be made of metallic materials with a large relative permeability; (3) notches should be placed in the center region of the exciting coil; (4) the depth of notches should be in the range of 4–8 mm; (5) a rhombic exciting coil could improve the identification of notches compared with a circular one; (6) a small exciting coil could improve the identification of notches compared with a large one; (7) a large exciting coil could enlarge the region in which a notch can be detected compared with a small one; (8) the anti-jamming ability of ACFM detection can

be improved by increasing the operating frequency; and (9) the pick-up coil should be placed close to the MBL as much as possible.

3.2 Identification of multi-notch MBLs

The parameters used in the simulations (Experiments 7 and 8) for the MBLs containing multiple notches are summarized in Table 2.

In Experiment 7, the identification of MBLs made of mild steel containing multiple notches with interval of 1 mm (y_n=−5, −4, −3, −2, and −1 mm, d=4 mm) is investigated. The MBLs are excited by a rhombic coil with l=21.5 mm and w=11.5 mm and the operating frequency f is 20 kHz. Fig. 9 gives the magnitude and phase of H_y along the pick-up coil's moving path obtained by simulation. The left inset shows the phase of H_y along the pick-up coil's moving path, and the right inset shows the detailed magnitude of H_y at the position of the notches. It is seen that one cannot distinguish notches with interval 1 mm by inspecting H_y directly without any additional signal processing.

In Experiment 8, the identification of MBLs made of mild steel containing multiple notches with interval 2 mm (y_n=−5, −3, −1 mm, d=4 mm) is investigated. The MBLs are excited by the same rhombic coil as that in Experiment 7. Fig. 10 gives the magnitude and phase of H_y along the pick-up coil's moving path, obtained by simulation. The left inset shows the phase of H_y along the pick-up coil's moving path, and the right inset shows the detailed magnitude of H_y at the position of the notches. It is seen that one can clearly distinguish notches in the center region (y_n=−3, −1 mm) with interval 2 mm by inspecting H_y directly, but at y_n=−5 mm, to locate the notches, additional signal processing is needed.

By the simulations of the multi-notch MBL (Figs. 9 and 10), one can obtain the distinguishable region and sensitivity of an MBL system, under the excitation of a rhombic inducer, which can be a reference in design.

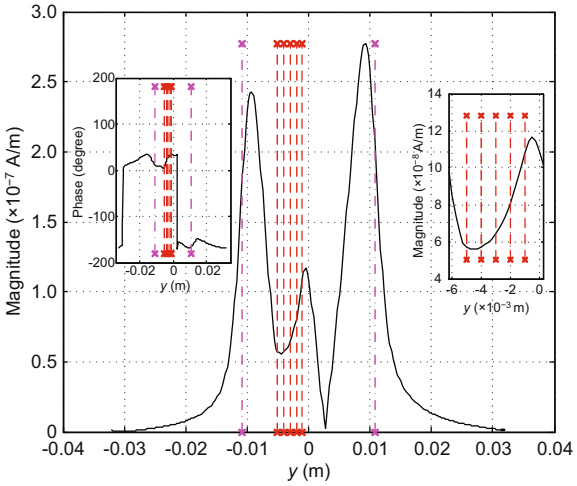

Fig. 9 Simulation results of H_y when a metal label contains five notches separated by 1 mm. The left inset shows the phase of H_y. The right inset shows the detailed magnitude of H_y at the position of the notch. The positions of the notches are marked with vertical dashed lines, and the position of the exciting coil is marked with vertical dash-dotted lines

4 Conclusions and future work

We employ the nondestructive evaluation involving AC field measurement in detecting and identifying metal barcode labels, providing reference for design. Using the magnetic scalar potential boundary condition at notches in thin-skin field theory and 2D Fourier transform, we provide an analytical model for the magnetic scalar potential induced by the interaction of the high-frequency inducer with a metal barcode label containing multiple narrow saw-cut notches and then the magnetic field in the free space above the metal barcode label. With the simulation of the magnetic field, qualitative analysis was given for the effects on detecting and

Table 2 Parameters used in the simulations for MBLs containing multiple notches

Experiment	Metal substrate material	Shape of the exciting coil	Operating frequency, f (kHz)	Lift-off distance, q (mm)	Notch depth, d (mm)	Notch position, y_n (mm)	Simulation results
7	Mild steel	Small rhombic coil	20	0.76	4	−5, −4, −3, −2, −1	Fig. 9
8	Mild steel	Small rhombic coil	20	0.76	4	−5, −3, −1	Fig. 10

Properties of the mild steel substrate material: μ_r=100, σ=6 × 10^6 S/m. Dimensions of the exciting rhombic coil: diagonals l=21.5 mm and w=11.5 mm. The exciting coil is placed at h=3.16 mm. Exciting current magnitude I_m=1 A. The openings of all the notches are g=150 μm

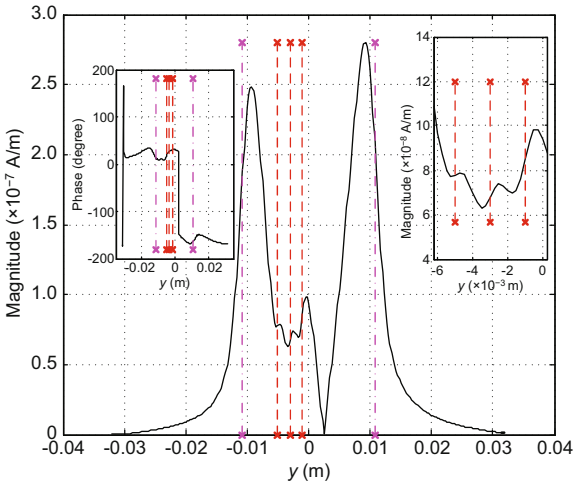

Fig. 10 Simulation results of H_y when a metal label contains three notches separated by 2 mm. The left inset shows the phase of H_y. The right inset shows the detailed magnitude of H_y at the position of the notch. The positions of the notches are marked with vertical dashed lines, and the position of the exciting coil is marked with vertical dash-dotted lines

identifying MBLs, which are caused by metal material, notch characteristics, exciting inducer properties, and other factors. These results (Section 3.1) can be used as a reference in metal barcode label design.

This paper gives a mathematical model for MBLs with narrow saw-cut notches. However, for a real MBL, to contain much more information bits, a notch may have a width compatible with its length and depth. This is the fundamental difference between MBL and NDE. It means that a mathematical model for a wide notch must be established, on which our further work will focus.

Acknowledgements

We thank Ze-heng KONG for providing the figures and Xiao-jun CAO for valuable comments.

References

Amineh, R.K., Ravan, M., Sadeghi, S.H.H., *et al.*, 2008. Using AC field measurement data at an arbitrary liftoff distance to size long surface-breaking cracks in ferrous metals. *NDT & E Int.*, **41**(3):169-177. http://dx.doi.org/10.1016/j.ndteint.2007.10.002

Auld, B.A., Moulder, J.C., 1999. Review of advances in quantitative eddy current nondestructive evaluation. *J. Nondestruct. Eval.*, **18**(1):3-36. http://dx.doi.org/10.1023/A:1021898520626

Bowler, J.R., 1994. Eddy-current interaction with an ideal crack. I. the forward problem. *J. Appl. Phys.*, **75**(12): 8128-8137. http://dx.doi.org/10.1063/1.356511

Bowler, J.R., Harfield, N., 1998. Evaluation of probe impedance due to thin-skin eddy-current interaction with surface cracks. *IEEE Trans. Magnet.*, **34**(2):515-523. http://dx.doi.org/10.1109/20.661483

Bowler, J.R., Sabbagh, L., Sabbagh, H., 1989. A theoretical and computational model of eddy-current probes incorporating volume integral and conjugate gradient methods. *IEEE Trans. Magnet.*, **25**(3):2650-2664. http://dx.doi.org/10.1109/20.24505

Bowler, J.R., Sabbagh, L.D., Sabbagh, H.A., 1990. Eddy-current probe impedance due to a surface slot in a conductor. *IEEE Trans. Magnet.*, **26**(2):889-892. http://dx.doi.org/10.1109/20.106460

Bowler, J.R., Theodoulidis, T.P., Poulakis, N., 2012. Eddy current probe signals due to a crack at a right-angled corner. *IEEE Trans. Magnet.*, **48**(12):4735-4746. http://dx.doi.org/10.1109/TMAG.2012.2203918

Ditchburn, R.J., Burke, S.K., Posada, M., 2003. Eddy-current nondestructive inspection with thin spiral coils: long cracks in steel. *J. Nondestruct. Eval.*, **22**(2):63-77. http://dx.doi.org/10.1023/A:1026340510696

Dodd, C.V., Deeds, W.E., 1968. Analytical solutions to eddy-current probe-coil problems. *J. Appl. Phys.*, **39**:2829-2838. http://dx.doi.org/10.1063/1.1656680

French, P.C., Bond, L.J., 1988. Finite-element modeling of eddy-current nondestructive evaluation (NDE). *J. Nondestruct. Eval.*, **7**(1):55-69. http://dx.doi.org/10.1007/BF00565777

Grimberg, R., 2011. Electromagnetic nondestructive evaluation: present and future. *Stroj. vestn. J. Mech. Eng.*, **57**(3):204-217.

Lewis, A.M., Michael, D.H., Lugg, M.C., *et al.*, 1988. Thin-skin electromagnetic fields around surface-breaking cracks in metals. *J. Appl. Phys.*, **64**:3777-3784. http://dx.doi.org/10.1063/1.341384

Michael, D.H., Waechter, R.T., Collins, R., 1982. The measurement of surface cracks in metals by using AC electric fields. *Proc. R. Soc. Lond. A*, **381**(1780):139-157. http://dx.doi.org/10.1098/rspa.1982.0062

Michael, D.H., Lewis, A.M., McIver, M., *et al.*, 1991. Thin-skin electromagnetic fields in the neighbourhood of surface-breaking cracks in metals. *Proc. R. Soc. Lond. A*, **434**(1892):587-603. http://dx.doi.org/10.1098/rspa.1991.0115

Mirshekar-Syahkal, D., Mostafavi, R.F., 1997. Analysis technique for interaction of high-frequency rhombic inducer field with cracks in metals. *IEEE Trans. Magnet.*, **33**(3):2291-2298. http://dx.doi.org/10.1109/20.573845

Morisue, T., 1982. Magnetic vector potential and electric scalar potential in three-dimensional eddy current problem. *IEEE Trans. Magnet.*, **18**(2):531-535. http://dx.doi.org/10.1109/TMAG.1982.1061856

Mostafavi, R.F., Mirshekar-Syahkal, D., 1999. AC fields around short cracks in metals induced by rectangular coils. *IEEE Trans. Magnet.*, **35**(3):2001-2006. http://dx.doi.org/10.1109/20.764900

Ostovarzadeh, M.H., Sadeghi, S.H.H., Moini, R., 2011. Field distributions around a long opening in a metallic half space excited by arbitrary-frequency alternating current-carrying wires of arbitrary shape. *IEEE Trans. Magnet.*, **47**(11):4600-4610. http://dx.doi.org/10.1109/TMAG.2011.2148176

Ostovarzadeh, M.H., Sadeghi, S.H.H., Moini, R., *et al.*, 2013. Field distributions around a rectangular crack in a metallic half-space excited by long current-carrying wires with arbitrary frequency. *IEEE Trans. Magnet.*, **49**(3):1108-1118. http://dx.doi.org/10.1109/TMAG.2012.2225440

Presser, M., Barnaghi, P.M., Eurich, M., *et al.*, 2009. The SENSEI project: integrating the physical world with the digital world of the network of the future. *IEEE Commun. Mag.*, **47**(4):1-4. http://dx.doi.org/10.1109/MCOM.2009.4907403

Ravan, M., Sadeghi, S.H.H., Moini, R., 2006. Field distributions around arbitrary shape surface cracks in metals, induced by high-frequency alternating-current-carrying wires of arbitrary shape. *IEEE Trans. Magnet.*, **42**(9): 2208-2214. http://dx.doi.org/10.1109/TMAG.2006.877655

Salemi, A.H., Sadeghi, S.H.H., Moini, R., 2004. Thin-skin analysis technique for interaction of arbitrary-shape inducer field with long cracks in ferromagnetic metals. *NDT & E Int.*, **37**(6):471-479. http://dx.doi.org/10.1016/j.ndteint.2003.12.002

Theodoulidis, T., Bowler, J., 2005. Eddy-current interaction of a long coil with a slot in a conductive plate. *IEEE Trans. Magnet.*, **41**(4):1238-1247. http://dx.doi.org/10.1109/TMAG.2005.844838

Theodoulidis, T., Bowler, J.R., 2010. Interaction of an eddy-current coil with a right-angled conductive wedge. *IEEE Trans. Magnet.*, **46**(4):1034-1042. http://dx.doi.org/10.1109/TMAG.2009.2036724

Tian, G.Y., Sophian, A., 2005. Reduction of lift-off effects for pulsed eddy current NDT. *NDT & E Int.*, **38**(4):319-324. http://dx.doi.org/10.1016/j.ndteint.2004.09.007

Tian, G.Y., Zhao, Z.X., Baines, R.W., 1998. The research of inhomogeneity in eddy current sensors. *Sens. Actuat. A*, **69**(2):148-151. http://dx.doi.org/10.1016/S0924-4247(98)00085-5

Xu, E.X., Simkin, J., 2004. Total and reduced magnetic vector potentials and electrical scalar potential for eddy current calculation. *IEEE Trans. Magnet.*, **40**(2):938-940. http://dx.doi.org/10.1109/TMAG.2004.824887

Zeng, Z.W., Liu, X., Deng, Y.M., *et al.*, 2007. Reduced magnetic vector potential and electric scalar potential formulation for eddy current modeling. *Przegl. Elektrotechn.*, **83**(6):35-37.

Zeng, Z.W., Udpa, L., Udpa, S.S., 2010. Finite-element model for simulation of ferrite-core eddy-current probe. *IEEE Trans. Magnet.*, **46**(3):905-909. http://dx.doi.org/10.1109/TMAG.2009.2034651

Zhou, J., Lugg, M.C., Collins, R., 1999. A non-uniform model for alternating current field measurement of fatigue cracks in metals. *Int. J. Appl. Electrom. Mech.*, **10**(3):221-235.